Published in final edited form as:
J Nucl Med Technol. 2011 June ; 39(2): 131–139. doi:10.2967/jnmt.110.081893.

Automated patient motion detection and correction in dynamic renal scintigraphy

Russell D. Folks, **Daya Manatunga**, **Ernest V. Garcia**, and **Andrew T. Taylor**
Emory University School of Medicine, Department of Radiology, Atlanta, GA

Abstract

Kidney motion during dynamic renal scintigraphy can cause errors in calculated renal function parameters. Our goal was to develop and validate algorithms to detect and correct patient motion.

Methods—We retrospectively collected dynamic images from 86 clinical renal studies (42 females, 44 males), acquired using the following protocol for ^{99m} Tc Mertiatide (MAG3) imaging: 80 128×128 image frames (24 2-second frames, 16 15-second frames, 40 30-second frames, 128×128, 3.2 mm/pixel). We simulated ten types of vertical motion in each patient study, resulting in 860 image sets. Motion consisted of up or down shifts of magnitude 0.25 pixels to 4 pixels per frame, and were either A) gradual shift additive over multiple frames or B) abrupt shift of one or more consecutive frames, with a later return to the start position. Additional horizontal motion was added to test its effect on detection of vertical motion. Original and shifted files were submitted to a motion detection algorithm. Corrective shifts were applied, and corrected and original, unshifted images were compared on a pixel by pixel basis. Motion detected in the shifted data was also tabulated before and after correcting for motion detected in the original unshifted data. A detected shift was considered correct if it was within 0.25 pixel of the simulated magnitude. Software was developed to facilitate visual review of all images, and to summarize kidney motion and motion correction using linograms.

Results—Overall detection of simulated shifts was 99% (3068/3096 frames) when the existing motion in the original images was first corrected. When the original motion was not corrected, overall shift detection was 76% (2345/3096 frames). For image frames in which no shift was added, (and original motion was not corrected) 87% (27142/31132 frames) were correctly detected as having no shift. When corrected images were compared to original, calculated count recovery was 100% for all shifts that were whole pixel magnitudes. For fractional pixel shifts, percent count recovery varied from 52–73%. Visual review suggested that some original, unshifted frames exhibited true patient motion.

Conclusions—The algorithm accurately detected motion as small as 0.25 pixels. Whole pixel motion can be detected and corrected with high accuracy. Fractional pixel motion can be detected and corrected but with less accuracy. Importantly, the algorithm accurately identified unshifted frames, which helps to prevent the introduction of errors during motion correction.

Keywords

motion correction; renal scintigraphy; cross-correlation

Address for Correspondence: Russell D. Folks, Department of Radiology, Emory University Hospital, 1364 Clifton Rd., NE, Atlanta, GA 30322, voice: 404-727-3805, fax: 404-727-3889, rfolks@emory.edu.

DISCLOSURE

Authors RDF, EVG and ATT receive royalties from sale of QuantEM software which is related to the software used in this project. This arrangement has been reviewed and approved by Emory University in accordance with its conflict-of-interest policy.

BACKGROUND AND OBJECTIVES

Body motion during imaging is an important cause of visual artifacts and reduced reliability of computerized, quantitative image analysis techniques in a number of imaging procedures. [1–13] The effects of motion can result from patient movement, normal respiration and normal cardiac motion.

Quantitative nuclear renography using ^{99m} Tc Mertiatide (MAG3) has been used for various clinical indications, including assessment of renal function[14], renal obstruction[15] and renovascular hypertension[16]. Using appropriate software, a number of functional parameters can be calculated, compared to normal ranges[17,18] and used for the diagnosis of obstruction and renovascular hypertension.

Patient motion is a concern in renography because of the relatively long acquisition time during which the patient is expected to remain still. Although any type of motion is possible, one common type is for the patient to slide toward the head or foot of the imaging table. Significant patient motion could potentially degrade the images and affect the slope of renal clearance curves. This happens most likely by reducing counts within the kidney regions, thus making an abnormal curve appear less abnormal. Motion could also adversely affect calculated parameters of renal function. For example, a change in the ratio of counts in the renal cortex at 20 minutes post injection to the maximum cortical counts (20 min/max ratio) of 0.15 or greater is a criterion for the diagnosis of renovascular hyptertension[19]. Motion at specific points during the study can distort the 20 min/max ratio measurement on either the baseline or post captopril scan and lead to an incorrect diagnosis. This potential for misdiagnosis indicates the need for motion detection, and correction. When there is marked patient motion and a correction algorithm is not available, a study may have to be repeated[20].

For a variety of imaging procedures, methods have been developed in other laboratories to monitor and correct motion, including the use of external radioactive point sources[21], optical sensors for patient monitoring[22], frame-to-frame tracking of image features[23], and manual correction of shifted frames. In recent years, sophisticated methods have been proposed to deal with body and respiratory motion in high-resolution imaging, in which small or complex image features will be segmented as part of standard processing [11,13,24]. There have been several methods reported for motion correction of radionuclide renograms. In 1992, De Agostini et al. reported a method for re-aligning shifted renogram images by using statistical methods to select from a set of shifted ROIs the one that best represents the motion of features within the image[25]. Lee and Barber used affine transformation with decomposition to motion correct renograms [26].

We previously reported the development of QuantEM-II[27], a quantitative nuclear renography software package which is an enhanced version of the commercial program QuantEM. A computerized decision support system (DSS) has been developed to aid in the interpretation of MAG3 scans in patients with suspected obstruction[28,29]. To optimize the accuracy of the DSS, which utilizes the quantitative output of QuantEM-II, it is necessary to monitor study quality, including patient motion. We have also reported the development of quality control (QC) software for use with QuantEM-II[30], although the QC software did not originally include an algorithm for patient motion detection.

Our main goal in this study was to develop and validate a simple, computerized method to automatically detect and correct patient motion in acquired images. We decided to base our method on frame to frame cross-correlation, a well-established technique that has been used previously to correct motion in cardiac SPECT[31] and in planar dynamic radionuclide studies[32] [33]. A secondary goal was to develop a method to conveniently review renal

studies before and after correction, by viewing sequential image frames as well as linograms, which allow the whole study to be summarized in a single image. The use of linograms to drive motion correction algorithms for SPECT has been reported by Wallis[34] and by Smith, et al.[35]

METHODS

Patient Population

We retrospectively collected 86 clinical ^{99m} Tc MAG3 renal studies. 76 patients were referred for evaluation of possible renal obstruction, and 10 were renal transplant donors. There were 42 females and 44 males, selected without regard to image quality or renal function. Subjects ranged in age from 18 to 87 years, with total MAG3 clearance from 25 to 475 ml/min/1.73 m^2. Difference between left and right kidney contribution to clearance ranged from 2 to 327 ml/min/1.73 m^2.

Images were acquired using one of two gamma cameras, having a circular field of view (G.E. Medical Systems), or rectangular field of view (Philips Medical Systems). The acquisition protocol consisting of 80 image frames (24 2-second frames, 16 15-second frames, 40 30-second frames), using a 128×128 pixel matrix, 3.2 mm per pixel. All studies were processed with QuantEM-II. Left and right whole kidney ROIs were defined automatically by software, using a threshold technique, with manual adjustment as necessary.

Motion Simulation

All software was developed using IDL (Interactive Data Language (ITT Visual Information Solutions, Boulder, CO)). To simulate vertical patient motion, software was developed to shift selected frames of the dynamic renal study by any desired amount. Ten types of vertical motion were defined, each having a specific combination of magnitude, direction and range of frames shifted, as summarized in Table 1. Each of the ten shifts were independently applied to each patient's dynamic study, resulting in 860 shifted image sets (86 patients × 10 shifts/patient). Shifts were only applied to the 30-second frames, so in any one patient study there were 40 frames that could be shifted, resulting in a total of 34,400 image frames (40 frames × 860 image sets). The 86 original unshifted files and the 860 files containing shifted frames were submitted to motion detection.

Additional horizontal motion was also simulated using a four pixel horizontal (x-direction) shift added to each frame that already had simulated y-direction motion. The horizontal shift was either leftward or rightward. All sets of images with both vertical and horizontal motion were submitted again for motion detection.

Motion Detection

The motion detection utilizes linear cross-correlation, an algorithm that characterizes the difference between mathematical functions. In this case the functions to be compared are count profiles through successive images in the dynamic sequence. In our implementation of cross-correlation, frame 41 (the first frame in the series to be examined) is the initial standard. As illustrated in Fig. 1, a tight box is generated around each kidney using the outer limits of the stored kidney ROIs. The counts from pixel rows within each box are summed through all columns within the region of the kidneys, producing a vertical count profile for frame 41. Frame 42 is then shifted vertically upwards (or "lagged", in the terminology of cross-correlation) in increments of 0.25 pixels (0.8 mm) from 0.25 to 4.0 pixels and then shifted vertically downwards by the same amounts. The profile for each shifted version of frame 42 is calculated and correlated to the profile in frame 41 by comparing the areas under

each curve. The lagged frame 42 profile which results in the minimum difference from frame 41 corresponds to the amount of motion that occurred between frames 41 and 42. After this determination, frame 42 becomes the standard of comparison for determining the shift in the next frame, and this process continues to the end of the set of frames.

The shift detection algorithm was applied to the original data (before any simulated shift was applied) and the detected motion was tabulated. The shift detection algorithm operates on immediately adjacent frames. Because small frame-to-frame shifts can accumulate to become large shifts, the cumulative shift from beginning to end of the 40 frames was also tabulated.

Motion detection was executed on image data with y-direction simulated motion, and on image data with both y-direction and x-direction motion. For each frame, the detected shift was tabulated as correct if it matched the true shift that was introduced within ± 0.25 pixel. Tabulation was done both with and without correction of the motion detected in the original data.

The inclusion of x-direction motion was not an attempt to identify the magnitude of the x-direction shift, but rather to determine the effect of simultaneous horizontal motion on the algorithm's ability to quantitatively characterize vertical motion.

Motion Correction

Image frames in which motion was detected were shifted in an attempt to correct the motion. To evaluate the accuracy of motion correction, we used the summed pixel count values in both kidneys. For every image frame included in the motion simulation, there are three summed pixel values: for the original frame (O), for the shifted frame (S) and for the corrected frame (C). The shifted error fraction (SEF) was defined as the sum of |S-O|/O for all frames that were motion shifted. The corrected error fraction (CEF) was defined as the sum of |C-O|/O for all shifted frames. The accuracy of motion correction was characterized by percent restoration of the original counts, defined as (SEF−CEF)/SEF * 100.

For visual assessment of motion, display software was developed to allow frame by frame and linogram review of all images before and after motion correction.

RESULTS

Motion in the original data before any shifts were applied

Motion detected in the original data, before artificial shifts were added, is summarized in Figs. 2 and 3. In 95% of original image frames (3263/3440), the frame-to-frame shift detected was less than 1 pixel (3.2 mm). A cumulative shift of 2 pixels or less was detected in 65% of patients (56/86), upward cumulative shift >2 pixels in 8% (7/86) of patients, and downward cumulative shift > 2 pixels in 27% (23/86) of patients.

Detection of shifted frames

Detection of any simulated shift was considered correct if the detected value was within ± 0.25 pixel of the true value, however for simulated 0.25 pixel shifts, we did not accept zero as a correct detection. Only 0.25 or 0.5 pixel detected shifts were considered correct in this case. Overall shift detection was 99% (3068/3096 frames) when motion in the original images was corrected.

All subsequent analysis was done without correcting for motion in the original data. With this condition, the overall detection of simulated shifts was 76% (2345/3096 frames). Motion detection was tabulated for all ten types of simulated motion. Detection was 74–80%

for whole pixel shifts of one to four pixels, 71–78% for various fractional pixel shifts, 72–81% for various abrupt shifts and 71–78% for various gradual, continuous shifts, as plotted in Fig. 4.

Detection of unshifted frames

For image frames in which no shift was added, 87% (27142/31132) were correctly detected as having no shift. This value was calculated *without* correcting motion in the original data, therefore it is negatively skewed. Visual review of all image sets before and after correction suggests that there is kidney motion in some of the original studies, particularly in frames near the end of the study.

Detection of shifted frames in the presence of horizontal motion

As shown in table 2, detection of vertical motion was affected minimally by the presence of horizontal motion. Average detection for six different abrupt shifts was 77% for vertical motion 73% for vertical plus horizontal motion. Detection for five different continuous (gradual) shifts averaged 76% for vertical motion only, and 75% for vertical plus horizontal motion.

Motion correction

Motion correction was applied to all frames for which there was a simulated shift. For the five shift types that included only whole pixel shifts, calculated recovery of original counts in each shifted frame, (SEF − CEF)/SEF * 100, was 100%. For fractional pixel shifts, recovery of original counts varied from 52–73%. Table 3 summarizes these results for all types of simulated motion that were applied.

Visual review tool

A sample display from the motion review tool is shown in Fig. 5. Images can be reviewed frame by frame before and after correction. Using a slider control, the images can be viewed in rapid succession, similar to a cine loop. The software also constructs linograms to represent the original and corrected data. The linogram is a static image consisting of 40 pixel columns. Each linogram column contains the sum of all pixel columns through both kidneys in the corresponding image frame. The linogram display summarizes the entire dynamic image set in a single static image, while highlighting the kidneys, which are the most important image feature. All studies were reviewed using the visual tool. Simulated motion could be easily seen in the uncorrected linograms, and was not evident, or much less evident, in the corrected linograms, as suggested by smoother superior and inferior boundaries of the kidneys.

DISCUSSION

We present a method for automatically detecting patient motion, which uses frame-to-frame correlation of counts in and adjacent to the whole-kidney regions of interest. Because kidney regions of interest (ROI) are defined on summed images from the 2–3 minute interval post-injection, which are somewhat blurred by respiratory motion, there is a certain amount of motion tolerance in the regions[20]. Motion of the body that occurs later than 3 minutes will shift the kidney away from the assigned ROI, which remains fixed for the duration of acquisition, and will reduce the counts within the kidney regions. A common motion compensation technique is to increase the size of the ROIs to avoid excluding kidney counts due to motion, however this may result in inappropriate background subtraction. In this study, all ROIs were defined based on the apparent size of the kidneys in the 2–3 minute

image, and were not enlarged. In our study, we employed a cross-correlation algorithm for motion detection, with the following enhancements:

1. We used the kidney ROI locations to identify the most important regions of the profile. The technique of segmenting essential image features by defining regions of interest, as a starting point to drive motion detection and correction, has been used previously in magnetic resonance (MR) renography[36–38].
2. We do not allow the cross-correlation to pad the profile with zeroes as the lags are introduced. The default behavior of the cross-correlation is to assume that, as the profile is shifted by each lag, zero values are added to the end of the profile to maintain the same number of data points. In our implementation, “real” pixel count values are pulled in from above and below the ROI location as the profile is shifted.
3. We use a moving reference frame, that is, the current profile is adjusted to best match the previous one, and then the current profile becomes the reference for the next frame.

These changes to the basic algorithm might be expected to lead to improved performance in motion detection, although the current study is not able to prove this since we did not compare to the results of another detection method. To test the method, we used images from clinical patients with a range of MAG3 clearances and a range of differential kidney function parameters. To simulate motion, we introduced image shifts of whole or fractional pixel amounts through various ranges of the 30-second frames. The threshold at which motion begins to significantly affect the confidence of scan interpretation is unknown, so we used shifts as small as 0.25 pixels (0.8mm) and as large as 4 pixels (12.8mm). The shift magnitudes, locations and durations simulate a variety of motions.

Motion that was present in the original images might bias the detection results. Pre-existing motion was probably not significant, since none of our studies had motion concerns noted on the clinical report. Most of the frame-to-frame motion detected in the original data was small, with 95% of the detected motion consisting of shifts of 1 pixel or less between adjacent frames.

Similarly, cumulative motion in the original data was usually less than two pixels. When it was greater than 2 pixels, a downward shift was three times more frequent than an upward shift. We hypothesized that this was due in part to clinically insignificant patient motion, and in part to the normal, downward excretion pattern of MAG3, which could conceivably confuse the detection algorithm. An example is shown in Fig. 6. Visual inspection of the linograms and sequential image frames suggested that both patient motion and excretory shift of tracer were present in the original studies.

We first corrected shifts detected in the original version of each image set prior to applying the motion detection algorithm. Shift detection was excellent under these conditions. This is a purposeful simulation, but it does not match the real world condition, in which the “original” shifts would not be known. Therefore, we also tabulated motion detection rate without correcting the original data, and this accounts for a reduction in shift detection rate from 99% under “ideal” conditions to the range of 71–81%.

For most simulated shifts, a tolerance of ± 0.25 pixel was allowed. For shifts of exactly 0.25 pixel, zero was not counted as a correct detection event. With this restriction, 79% of the smallest, 0.25 pixel shifts were correctly detected. Detection of vertical motion was always in the range of 70–80%, even in the presence of significant (4 pixel) horizontal motion.

It is important that a motion detection algorithm should not detect motion where none is present. In this study there were 34,400 image frames (86 patients * 40 frames * 10 shift types, excluding the original unmodified data). Of this total, 31,132 image frames did not receive a simulated shift, and 87% of these were correctly identified as having no shift. This tabulation was done on data without correction of the original motion that was present. Some of the remaining 13% of frames probably had true patient motion (not clinically significant) and some frames exhibited significant movement of the radiotracer between frames, related to excretion, as suggested by visual review.

Motion correction was applied to all frames that had a simulated shift. In the case of whole pixel simulated shifts, there was complete recovery of the original pixel counts. By comparison, count recovery of fractional pixel shifts (table 2) was less, but still occurred in the majority of cases.

Pixel count values are interpolated when the fractional simulated shift is applied, and are interpolated again during correction; each interpolation creates a small error or uncertainty in many pixels and this error largely accounts for the reduced correction of the fractional-pixel shifts. Variability in the accuracy of shift correction between one shift type and another appears to be determined in part by how many pixels have a fractional shift and whether the shift back to the starting position is a whole pixel or a fractional pixel amount. While percent count recovery is an objective metric that allows comparison of motion correction performance with different types of simulated motion, it is not possible to achieve 100% accuracy in count recovery in the case of fractional pixel shifts, using the current algorithm. Thus, percent recovery probably underestimates the performance of the algorithm in improving images affected by motion.

In clinical studies, it is likely that spontaneous patient motion would involve fractional pixel amounts. Furthermore, pixel interpolation is not unlike the blurring that would occur if the patient moves at some arbitrary time during the 30 second frame. The estimate of detection and correction suggested by our results predict a very acceptable “real world” performance for the methodology.

To visually evaluate the performance of our method, software was developed to display the image frames as well as linograms representing the entire uncorrected and corrected studies, each in a single image. This is a user friendly approach, since the linogram columns are essentially count profiles of each image frame, similar to the count profiles on which the cross-correlation operates. The linograms provided a simple and straightforward visual method to detect renal motion and evaluate the correction algorithm. However care must be taken to judge the corrected linogram by the activity along the edges of the kidneys, rather than by the smoothness of the whole linogram image. Pixel interpolation is similar to a mild image filter, which might make the corrected linogram image appear slightly smoother, whether or not motion is appropriately corrected.

Study Limitations

We examined only the 30-second frames for motion. Motion that occurs prior to the 30-second frame acquisition (5 minutes in the protocol used) would not be detected. For each study, there was a single instance of simulated motion, over a small number of frames, always with an eventual return to the start position.

Our method may not be applicable to all cases of motion in pediatric studies. Children sometimes exhibit movement which is different than that seen in adult patients[12,39]. None of our subjects were less than 18 years of age. Only patients referred for evaluation of

possible renal obstruction, or for evaluation of renal function before kidney donation for transplant were included in the study.

We assume that the area most useful for motion detection includes both kidney ROIs. If there is significant unilateral or bilateral decreased kidney function, there will be reduced radiopharmaceutical uptake in the kidneys, with higher background. A few such cases were included in the study group, and motion detection was not systematically degraded in these kidneys.

Visual review of the images was not conducted by independent observers. This step should be included in any clinical test of the motion correction methodology. Finally, it remains to be demonstrated that (1) the motion simulated and detected in our test is the type and magnitude that adversely affects the calculation of renogram parameters and subsequent interpretation of the renogram, and (2) that the motion correction algorithm can correct the errors in the parameter values and restore the original renogram interpretation. This issue might be best addressed by our expert system software[28] but further investigation is required.

Future Directions

The cross-correlation algorithm depends on adequate signal-to-noise ratio, particularly if object shapes change between frames, as is expected in renography. If renal function is reduced, the method may benefit from background subtraction[31], examining left and right kidneys separately, or including counts from an area broader than boxes around the kidney ROIs.

With further validation, the motion detection program can be incorporated into our overall QC module to correct functional parameter values, so that the data transmitted to our decision support system will lead to more accurate scan interpretation.

CONCLUSIONS

The motion detection algorithm accurately identified artificially simulated motion of as little as 0.25 pixels (0.8mm). The detection rate was maintained whether the shifts were upward or downward, gradual or abrupt, and was also maintained when both vertical and horizontal motion were applied to the same frames. Whole pixel vertical motion can be precisely corrected, but fractional pixel motion can only be partially corrected due to imprecision introduced by pixel interpolation. Importantly, the motion detection algorithm accurately identified frames which were not shifted, which should minimize the introduction of artifact caused by attempting to “correct” frames that do not need correction.

Acknowledgments

This work was supported by grant R01- EB008838 from The National Institute of Biomedical Imaging and Bioengineering (NIBIB) and the National Institute of Diabetes and Digestive and Kidney Diseases (NIDDK).

References

1. Cooper J, Neumann P, McCandless B. Effect of patient motion on tomographic myocardial perfusion imaging. J Nucl Med. 1992; 33:1566–1571. [PubMed: 1634955]
2. Prigent F, Hyun M, Berman D, Rozanski A. Effect of motion on thallium-201 SPECT studies: A simulation and clinical study. J Nucl Med. 1993; 34:1845–1850. [PubMed: 8229222]
3. Wang Y, Riedered S, Ehman R. Respiratory motion of the heart: Kinematics and the implications for the spatial resolution in coronary imaging. Magn Reson Med. 1995; 33:713–719. [PubMed: 7596276]

4. Zuo C, Jiang A, Buff F, Mahon T, Wong T. Automatic motion correction for breast MR imaging. Radiology. 1996; 198:903–906. [PubMed: 8628891]
5. Mijailovich S, Treppo S, Venegas J. Effects of lung motion and tracer kinetics corrections on PET imaging of pulmonary function. J Appl Physiol. 1997; 82:1154–1162. [PubMed: 9104852]
6. Chuang M, Hibberd M, Beaudin R, et al. Patient motion compensation during transthoracic 3-D echocardiography. Ultrasound Med Biol. 2001; 27:203–209. [PubMed: 11316529]
7. Boucher L, Rodrigue S, Lecomte R, Benard F. Impact of respiratory motion on cardiac quantification with PET [abstract]. J Nucl Med. 2001; 42:165P.
8. Sance R, Ledesma-Carbayo M, Lundervold A, Santos A. Alignment of 3D DCE-mri abdominal series for optimal quantification of kidney function. Proceedings of the 5th International Symposium on Image and Signal Processing and Analysis. 2007:413–417.
9. Beegle C, Le Meunier L, Jones J, Maass-Moreno R, Bacharach S. Magnitude and direction of abdominal organ displacement at end-expiration and end-inspiration during PET/CT acquisitions [acstract]. J Nucl Med. 2005; 46:502P. [PubMed: 15750165]
10. Dhanantwari A, Stergiopoulos S, Iakovidis I. Correcting organ motion artifacts in x-ray CT medical imaging systems by adaptive processing. I. Theory. Med Phys. 2001; 28:1562–1576. [PubMed: 11548927]
11. Lyatskaya Y, Rehfeld K, Killoran J, Cormack R, Allen A. Su-ff-j-84: An algorithm for automated organ motion evaluation based on 4dct image analysis [abstract]. Med Phys. 2007; 34:2387.
12. Meadows A, Hogg P. An analysis of motion correction for $^{99}tc^{m}$ DMSA renal imaging in paediatrics. Radiography. 2007; 13:109–121.
13. Song T, Lee V, Rusinek H, Kaur M, Laine A. Automatic 4-D registration in dynamic MR renography based on over-complete dyadic wavelet and fourier transforms. Med Imge Comput Comput Assist Interv. 2005; 8:205–213.
14. Blaufox M, Aurell M, Bubeck B, et al. Report of the radionuclides in nephrourology committee on renal clearance. J Nucl Med. 1996; 37:1883–1890. [PubMed: 8917197]
15. Kalkman E, Paterson C. Radionuclide imaging of the renal tract: Principles and applications. Imaging. 2008; 20:23–28.
16. Taylor A, Nally J, Aurell M, et al. Consensus report on ACE inhibitor renography for detecting renovascular hypertension. J Nucl Med. 1996; 37:1876–1882. [PubMed: 8917196]
17. Esteves FPTA, Manatunga A, Folks RD, Krishnan M, Garcia EV. Normal values for camera-based 99mtc -MAG3 clearance, MAG3 curve parameters, excretory parameters and residual urine volume. AJR. 2006; 187:W610–W617. [PubMed: 17114514]
18. Lin W, Changlai S, Kao C. Normal ranges of renal physiological parameters for technetium-99m mercaptoacetyltriglycine and the influence of age and sex using a camera-based method. Urologia Internationalis. 1998:60.
19. Esteves F, Taylor A, Manatunga A, Folks R, Krishnan M, Garcia E. Normal values for camera-based ^{99m}tc -MAG3 clearance, MAG3 curve parameters, excretory parameters and residual urine volume. AJR. 2006; 187:W610–W617. [PubMed: 17114514]
20. Prigent A, Cosgriff P, Gates G, et al. Consensus report on quality control of quantitative measurements of renal function obtained from the renogram: International consensus committee from the scientific committee of radionuclides in nephrourology. Seminars in Nucl Med. 1999; 29:146–159.
21. Groch M, Erwin W, Turner D, Domnanovich J. Dual-isotope motion correction technique for gated exercise scintigraphy. J Nucl Med. 1985; 26:1478–1484. [PubMed: 4067647]
22. Fulton R, Meikle S, Eberl S, Pfeiffer J, Constable C, Fulham M. Correction for head movements in positron emission tomography using an optical motion-tracking system. IEEE Trans Nucl Sci. 2002; 49:116–123.
23. O'Connor M, Kanal K, Gebhard M, Rossman P. Comparison of four motion correction techniques in SPECT imaging of the heart: A cardiac phantom study. J Nucl Med. 1998; 39:2027–2034. [PubMed: 9867136]
24. Raghunath N, Faber T, Suryanarayanan S, Votaw J. Motion correction of PET brain images through deconvolution: Ii. Practical implementation and algorithm optimization. Phys Med Biol. 2009; 54:813–829. [PubMed: 19131667]

25. De Agostini A, Moretti R, Belletti S, Maira G, Magri G, Bestagno M. A motion correction algorithm for an image realignment programme useful for sequential radionuclide renography. Eur J Nucl Med. 1992; 19:476–483. [PubMed: 1644104]
26. Lee K, Barber D. Automatic motion correction in dynamic radionuclide renography using image registration. Nucl Med Commun. 1998; 19:1159–1167. [PubMed: 9885806]
27. Folks RDGE, Taylor AT. Development of a software application for quantitative processing of nuclear renography [abstract]. J Nucl Med. 2008; 49:157P.
28. Garcia EV, Taylor A, Halkar R, et al. RENEX: An expert system for the interpretation of 99mtc-MAG3 scans to detect renal obstruction. J Nucl Med. 2006; 47:320–329. [PubMed: 16455639]
29. Taylor A, Garcia E, Binongo J, et al. Diagnostic performance of an expert system for interpretation of Tc-99m MAG3 scans in suspected renal obstruction. J Nucl Med. 2008; 49:216–224. [PubMed: 18199609]
30. Folks RDGE, Taylor AT. Development and prospective evaluation of an automated software system for quality control of quantitative Tc-99m MAG3 renal studies. J Nucl Med Technol. 2007; 35:27–33. [PubMed: 17337654]
31. Eisner R, Noever T, Nowak D, et al. Use of cross-correlation function to detect patient motion during SPECT imaging. J Nucl Med. 1987; 28:97–101. [PubMed: 3491888]
32. Collins P, Leonard D, Chatterton B. Automatic correction for motion artefacts in dynamic radionuclide studies using a cross-correlation method [abstract]. J Nucl Med. 1993; 34:125P.
33. Georgiou M, Sfakianakis G, Nagel J, Cideciyan A. Patient motion compensation for renal scintigraphic studies by a fast correlation image registration method. J Nucl Med. 1994; 35:34P.
34. Wallis J. Use of the selective linogram for correction of patient motion in cardiac SPECT [abstract]. J Nucl Med. 1995; 36:168P.
35. Smith K, Tran H, Colucci K, et al. Vector evaluation of a SPECT motion correction algorithm which corrects horizontal and vertical motion separately using both the sinogram and linogram. J Nucl Med. 2004; 45:490P.
36. Sun, Y.; Jolly, M-P.; Moura, J. Integrated registration of dynamic renal perfusion MR images. IEEE International Symposium on Image Processing, ICIP'04; 2004; Singapore.
37. Zollner F, Sance R, Rogelj P, et al. Assessment of 3D DCE-mri of the kidneys using non-rigid image registration and segmentation of voxel time courses. Comput Med Imaging Graph. 2009; 33:171–181. [PubMed: 19135861]
38. Song T, Lee V, Chen Q, Rusinek H, Laine A. An automated three-dimensional plus time registration framework for dynamic MR renography. J Vis Commun Image Represent. 2010; 21:1–8.
39. Cooper J, McCandless B. Detection and correction of patient motion during tomographic imaging with DMSA [abstract]. J Nucl Med. 1995; 36:33P.

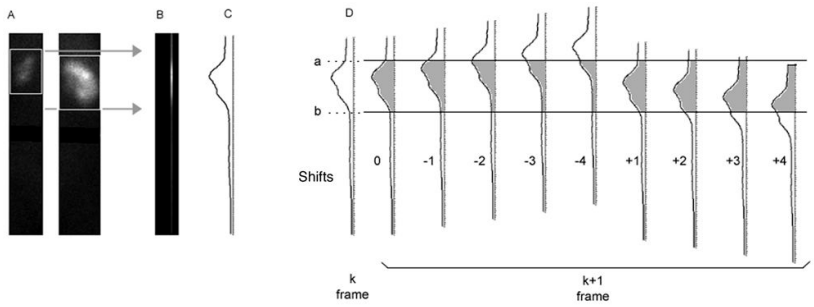

FIGURE 1.

Columns of pixels are summed across the width of each whole kidney box, 128 pixels from top to bottom of the image matrix (A). The area of the two kidneys is bounded by the top of the uppermost box and the bottom of the lowermost box, as shown by the gray arrows. The pixel columns are summed into a single column (B), in which the brightest area reflects counts from both kidneys. The summed column can be represented by a count profile (shown vertically in C), and the profile for each frame is then compared. Panel D shows frame to frame shift detection, with frame k as the initial reference frame. The height of the kidneys, from a to b, defines an area under the curve representing the total counts in the kidneys in this frame. Using the same a and b locations, frame k+1 is shifted upward 0 to 4 pixels, and downward 1 to 4 pixels, in 0.25 pixel increments. Count total is taken from a to b, and compared to the total from k. The shift amount (lag) corresponding to the total that most closely matches k gives the shift of k+1.

Since the lag can be as small as 0.25, the predicted location of frame k+1 is determined to within 0.25 pixel. k+1 then becomes the reference for frame k+2, and the sequence is repeated.

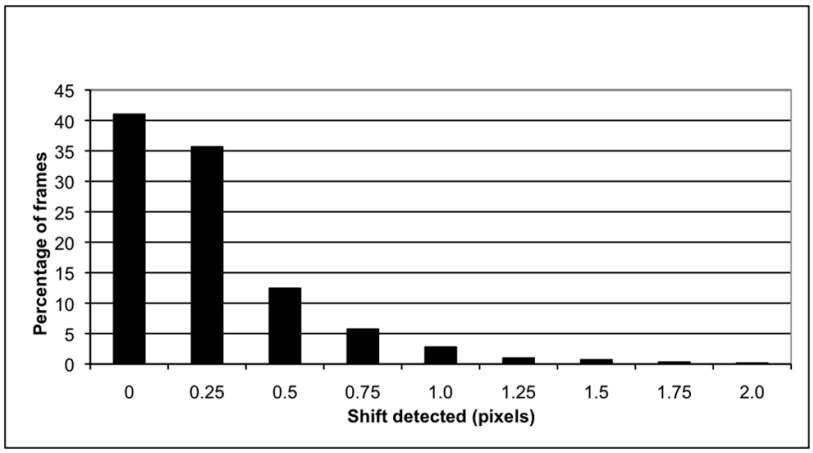

FIGURE 2.
Detection of shifts in the original images, before artificial shifts are introduced.

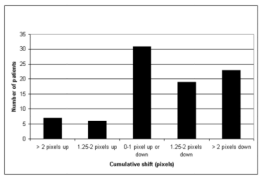

FIGURE 3.
Detection of cumulative shift, over any range of frames in the original data, before artificial shifts are introduced.

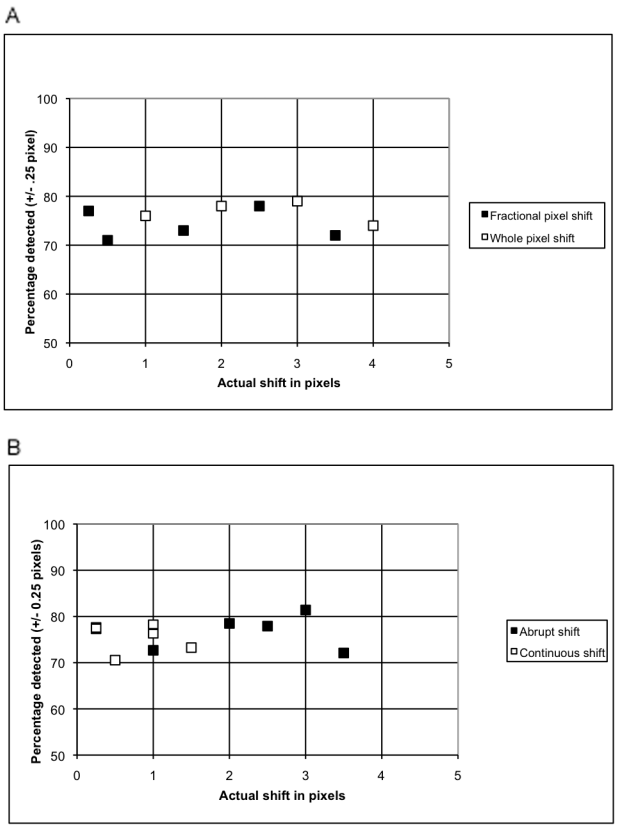

FIGURE 4.

Detection of simulated shifts of various types and magnitudes. Shifts present in the original data are not subtracted. Panel A plots the % motion detected for the fractional and whole pixel shifts while Panel B shows the % motion detected for the abrupt and continuous shifts.

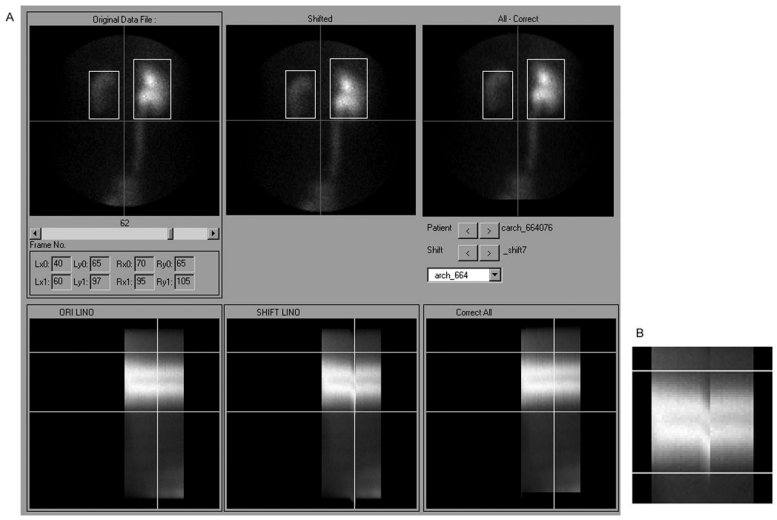

FIGURE 5.

An example patient study shown in the visual motion review tool. Below each kidney image in panel A is a corresponding linogram for the original unshifted images (left column), images with simulated shift (center column) and motion corrected images (right column). A slider control allows review of any image frame, and the current frame position is indicated by a vertical line on all linograms. Panel B shows an enlarged view of the linogram with image shifts, without the vertical line marker. This tool allows the user to select any of the 86 patients, and any of the ten artificial shifts, for visual comparison of uncorrected and corrected images and linograms.

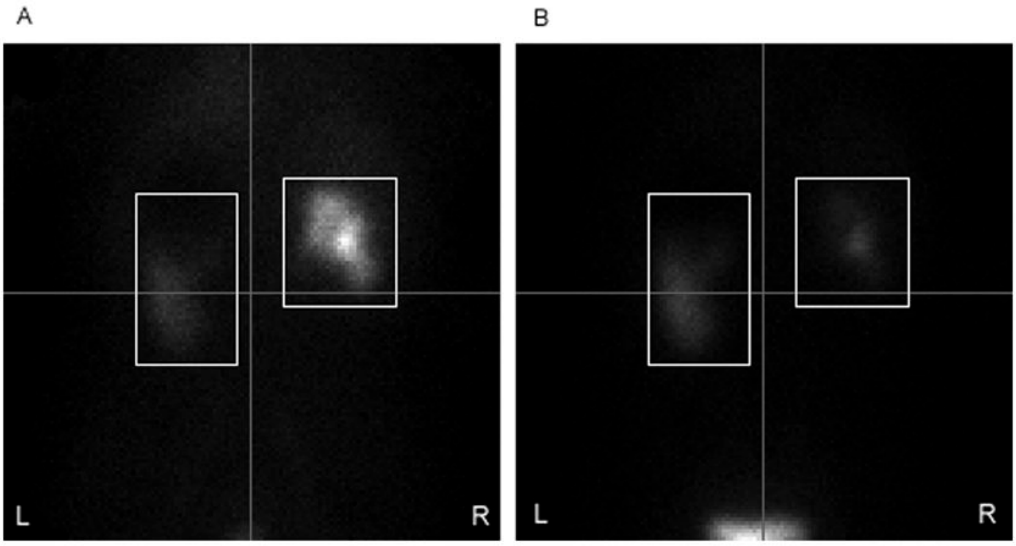

FIGURE 6.

Image frames from 4 minutes post injection of MAG3 (A), and 24 minutes post injection (B). The image in A is the first frame of the range submitted to motion detection, and in this patient there is little uptake of MAG3 in the left kidney at 4 minutes. In the profile generated by summing pixel columns in both kidneys, most of the counts are contributed by the right kidney, causing the profile peak to be nearer the top. By the time of image B, the right kidney has excreted MAG3 into the bladder, so more of the counts in the profile are contributed by the left kidney, which retains MAG3. The profile peak is thus lower than in A, which may falsely imply that vertical motion has occurred.

TABLE 1

Simulated shifts introduced into the image frames.

abrupt shifts	min shift	max shift	start frame	number of frames	initial shift	return shift
whole pixel	1	1	44	7	↑	↓
	3	3	59	2	↓	↑
	2	2	64	7	↑	↓
fractional	2.5	2.5	59	7	↓	↑
	3.5	3.5	78	2	↑	↓
gradual shifts						
whole pixel	1	4	59	5	↓	↑
	1	3	69	4	↑	↓
fractional	0.25	1.5	59	7	↑	↓
	0.5	3	49	7	↑	↓
	0.25	1	59	5	↓	↑

↑ = shift up ↓ = shift down

J Nucl Med Technol. Author manuscript; available in PMC 2012 June 1.

TABLE 2

Detection of simulated motion (% of frames shifted)

shift magnitude	**fractional pixel shift, y**	**fractional pixel shift, y+x**	**shift magnitude**	**whole pixel shift, y**	**whole pixel shift, y+x**
0.25	77	76	1	76	76
0.5	71	70	2	78	76
1.5	73	73	3	79	72
2.5	78	70	4	74	74
3.5	72	73			
shift magnitude	abrupt shift, y	abrupt shift, y+x	shift magnitude	continuous shift, y	continuous shift, y+x
1	73	73	0.25	77	76
2	78	76	0.5	71	70
2.5	78	70	1	77	77
3	81	73	1.5	73	73
3.5	72	73			

y = vertical motion, y+x = vertical plus horizontal motion

J Nucl Med Technol. Author manuscript; available in PMC 2012 June 1.

TABLE 3

Percent count recovery* (CR) after motion correction.

	Shift 4	Shift 5	Shift 6	Shift 8	Shift 10
Mean %CR	59.8	72.8	59.8	51.7	51.6
Std. Dev. %CR	7.2	7.5	12.8	13.5	16.8
Max %CR	75.8	86.7	83.8	72.4	69.0
Min %CR	42.0	50.9	20.4	14.2	0.0

*100% CR implies that the counts in the kidney ROI after motion correction are the same as before the motion took place.